RSC Advances

PAPER

View Article Online
View Journal | View Issue

Cite this: *RSC Adv.*, 2014, **4**, 42899

One-pot controlled synthesis of single-crystal α-Fe_2O_3 hollow nanostructure and its gas sensing properties†

Xiao Jia,[a] Fang Yue,[a] Xiang Chen,[a] Hai-Bo Pan,[a] Wen-Ge Liu*[b] and Jian-Yong Liu*[a]

Received 18th July 2014
Accepted 3rd September 2014

DOI: 10.1039/c4ra07275h

www.rsc.org/advances

A series of single-crystal α-Fe_2O_3 nanostructures with tunable morphologies have been prepared *via* a simple one-pot solvothermal synthesis. The as-prepared nanoparticles were fully characterized using X-ray diffraction (XRD), transmission electron microscopy (TEM), high-resolution TEM (HR-TEM), selective area electron diffraction (SAED), N_2 adsorption–desorption isotherms, and other techniques. The morphologies of the products can be easily adjusted by controlling the amount of NaAc added; with the amount of NaAc increasing the shell thickness of hollow spheres decreases, till the hollow structures disappeared and changed to nanoflower aggregates. Reaction temperature and the solvent ratio also play important roles in the synthesis of hollow nanospheres. The gas sensing properties of the as-prepared samples were also investigated. The results showed that the samples exhibited good gas sensing properties towards acetone vapor, and the gas sensing behavior was related to the morphologies of the samples.

1. Introduction

Hollow nanospheres with unique cavity structure have attracted a great deal of attention because of their wide variety of applications in the delivery and controlled release of drugs, selective absorption, catalysis and so on.[1,2] To date, the general approach for preparation of hollow nanostructures has involved the use of various templates, including hard templates (*e.g.* monodisperse silica particles and polymer latex colloids),[3–6] and soft templates (*e.g.* emulsion droplets/micelles, surfactant and gas bubbles).[7–11] However, the template method usually need tedious procedures (calcination *etc.*), thus a simple synthetic approach for controlled preparation of hollow nanostructures would be more preferred. As a result, template-free method using specific approaches such as Kirkendall effect and Ostwald ripening has been developed for the synthesis of various metal, metal oxide hollow particles *etc.*[12–17]

As the most stable iron oxide under ambient conditions, α-Fe_2O_3 (hematite) has a favorable optical band gap ($E_g = 2.1$ eV), and is widely used in catalysts, optical devices, sensors and pigments *etc.*[18–20] α-Fe_2O_3 nanostructures with a hollow interior often behave superior physicochemical properties as a result of the porous shells and high surface areas. Many groups have developed fabrication methods for the synthesis of α-Fe_2O_3 hollow particles. However, it is still a challenge to the one-step controlled synthesis of α-Fe_2O_3 hollow spheres as a result of the easy hydrolysis of iron ions. Aqueous media in the presence of structured micelles has been usually used in synthesizing α-Fe_2O_3 hollow morphology. But it is usually difficult to control the hydrolysis and polymerization kinetics of the iron ions in aqueous media, and product obtained by this method frequently suffer from relatively poor crystallinity, and often need a subsequent calcination process.[21–28]

In this report we successfully achieved the controlled synthesis of α-Fe_2O_3 hollow nanospheres *via* a simple, environmentally friendly one-step process. Nonaqueous solution method is a good way to separate nucleation and growth stages facilely, and high-quality product can be usually obtained.[29–32] Moreover, Chen and co-workers have demonstrated that the existence of water molecules can contribute to the dissolution–recrystallization process for the synthesis of hollow α-Fe_2O_3 nanospheres.[33] Based on this idea, we proposed a novel reaction system in which the water molecules were not initially introduced, but slowly formed during the reaction. In our system, long-chain hydrophobic alcohols that can dehydrate over a certain temperature were employed as reaction solvents. By making full use of the slow dehydration of long-chain hydrophobic alcohols solvents, not only the fast hydrolysis and polymerization problem can be solved, but also the dissolution–recrystallization of precursor can be facilitated that caused by the produced water molecules, and leading to the controlled synthesis of α-Fe_2O_3 hollow nanospheres eventually. As a result, α-Fe_2O_3 hollow nanospheres with tunable morphology can be

[a]*College of Chemistry, Fuzhou University, Fuzhou 350002, P. R. China. E-mail: liujianyong82@163.com; Tel: +86 591 87892632*

[b]*Department of Orthopedics, Affiliated Union Hospital of Fujian Medical University, Fuzhou 350001, P. R. China. E-mail: 13705977551@163.com; Tel: +86 591 83357896*

† Electronic supplementary information (ESI) available. See DOI: 10.1039/c4ra07275h

synthesized *via* one-pot process without calcinations. The design reflects the ability of controlled synthesis of compounds through artificially construct reaction system, and we believe the novel system can provide new ideas in the controlled synthesis of other metal oxide hollow spheres.

Furthermore, the gas sensing properties of both as-prepared samples and commercial sample were investigated. The results indicated that the as-prepared samples showed dramatically enhanced sensor sensitivity compared with the commercial sample. And all the as-prepared samples exhibited better gas sensing property to acetone vapor over other gases, which suggested the sensors have a potential application in acetone detection.

2. Experimental section

2.1 Synthesis

All chemicals were of analytical grade and used without further purification. In a typical synthesis process, 0.30 g of $FeCl_3$ and 0.20 g of NaAc were dissolved in a mixture of 12 mL *n*-octanol and 8 mL ethanol. The solution was then transferred into a 25 mL Teflon-lined stainless steel autoclave, kept at 220 °C for 4 h, and then cooled naturally. The product was separated by centrifugation, and washed with anhydrous ethanol and deionized water several times, and dried in air at 60 °C for 1 h.

2.2 Characterization

The crystal structure of the products were determined by the X-ray diffraction (XRD) patterns collected on a Rigaku D/Max 2200 PC diffractometer with a graphite monochromator and CuKα radiation ($\lambda = 0.15418$ nm). The morphology and microstructure were characterized using a high-resolution TEM (HRTEM, Tecnai G2 F20 S-TWIN, 200 kV) and SEM (Nova NanoSEM 230). The surface area of the products was measured by a BET (Brunauer–Emmett–Teller) method with N_2 adsorption–desorption on a gas adsorption analyzer (Autosorb-1, Quantachrome Corp., USA). The magnetic properties of the samples were determined on a SQUID (Quantum Design, MPMSXL-7) magneto-meter.

2.3 Fabrication of gas sensors and measurements of the gas sensing performance

The gas sensing performance was detected using a Gas Sensing Measurement System (JF02E, Jinfeng Tech. Co. Ltd., Kunming, China), and a gas calibration system incorporating mass flow controller set. The as-prepared samples were mixed with terpineol, and the obtained suspensions were spreaded on the alumina substrates. After drying in air for 2 days at room temperature, the film sensors were annealed at 300 °C for 2 h, and then aged at 300 °C in the gas sensing measurement system for a week before analysis.

3. Results and discussion

The crystalline structures of α-Fe_2O_3 hollow spheres were examined by XRD. Fig. 1b shows the XRD of the sample

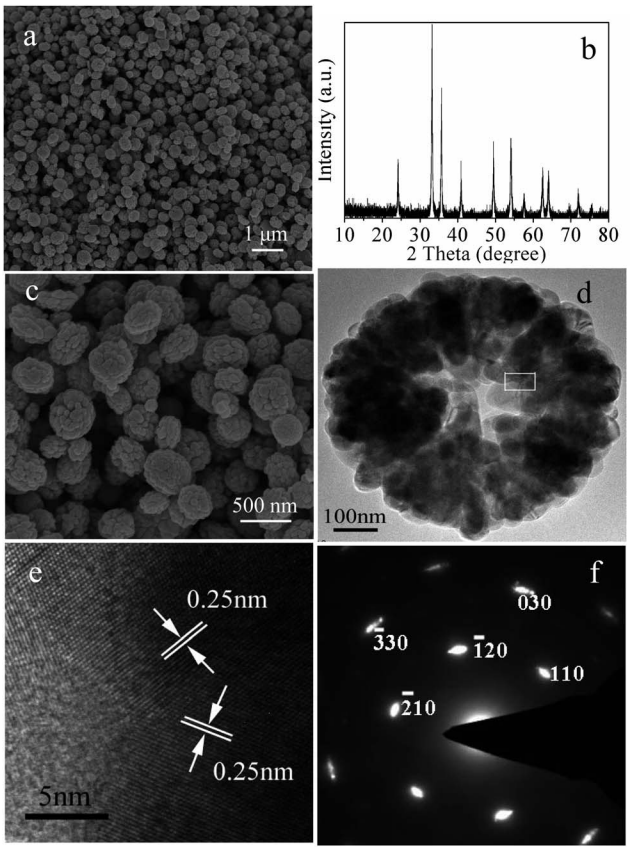

Fig. 1 SEM and TEM images of α-Fe_2O_3 hollow spheres in a typical synthesis. (a) Low-, and (c) high-magnification FESEM images of α-Fe_2O_3 hollow spheres; (b) a typical XRD pattern of α-Fe_2O_3 hollow spheres. (d) High-magnification TEM image of an individual hollow sphere; (e) HRTEM image obtained from the boxed area shown in (d) and (f) SAED pattern taken from the individual hollow sphere.

synthesized in a typical experiment. All the diffraction peaks can be well indexed to rhomb-centered α-Fe_2O_3 (JCPDS 33-0664). The average particle sizes for the sample are estimated to be 38.3 nm from Scherrer's formular. But SEM and TEM images in Fig. 1 show the hollow spheres are nearly 400 nm, which indicate the hollow spheres are constructed by small nanoparticles. Fig. 1a shows a low-magnification FESEM image of as-synthesized α-Fe_2O_3 products, which suggests that the product consists of a large number of spheres with an average diameter of *ca.* 400 nm. The magnified image in Fig. 1c indicates the α-Fe_2O_3 spheres are uniform, and some broken spheres exist, which confirm the spheres have a hollow interior. An individual hollow sphere provided more detailed structural information. The pale color regions in the central parts are in contrast to the dark edges in Fig. 1d, indicating a hollow structure of α-Fe_2O_3, and clearly revealing that the hollow sphere is constructed by several blocks. Fig. 1e shows the HRTEM image obtained from the boxed area in Fig. 1d, and the interlayer distance was calculated to be 0.25 nm, which agrees well with the (110) lattice plane of α-Fe_2O_3. Fig. 1f presents the SAED patterns of an individual hollow sphere shown in Fig. 1d, and gives the [001] zone axis spots characteristic of a α-Fe_2O_3 single-crystal,[34] which

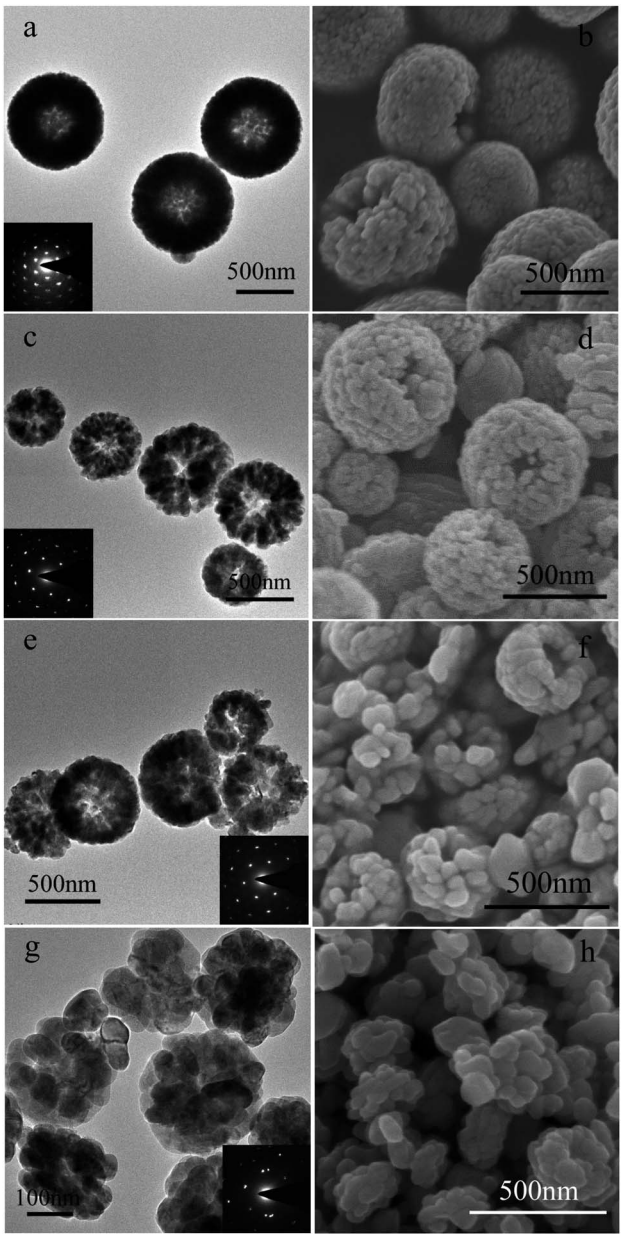

Fig. 2 Representative TEM images (a, c, e and g) and the corresponding SEM images (b, d, f and h) of α-Fe_2O_3 hollow spheres with adding different amounts of NaAc: 0.06 g (a and b), 0.12 g (c and d), 0.20 g (e and f), 0.26 g (g and h). The insets are the corresponding SAED patterns.

caused by oriented assembly. The nearest five spots can be indexed to (110), (030), (−120), (−210) and (−330) planes of α-Fe_2O_3.

Controlled synthesis of α-Fe_2O_3 hollow spheres can be obtained by adjusting the amount of NaAc added. As TEM images shown from Fig. 2a to g, it can be seen that increasing the amount of NaAc from 0.06 g to 0.26 g, there is a continuous decrease of shell compactness of hollow spheres (from Fig. 2a to e), till the hollow structures disappear (Fig. 2g). The shell thickness of hollow spheres are built up from dense particle aggregation to loose particle aggregation gradually, and in Fig. 2e some hollow spheres have broken, with a small amount of particle debris around. Broken spheres can be clearly seen in SEM images in Fig. 2b, d and f, which further confirm the hollow structures. When increasing the amount of NaAc to 0.26 g, nanoflowers built of several nanoparticles formed instead of the hollow structures, as shown in Fig. 2g and h. All TEM and SEM images indicated the hollow spheres or nanoflowers structures are formed by the assembly of small nanoparticles with diameter of tens of nanometers. The corresponding SAED patterns insets indicated all the samples behave single-crystal nature as a result of oriented aggregation.

In order to investigate the formation mechanism of the α-Fe_2O_3 hollow spheres, a detail time-dependent experiment was conducted at 220 °C. SEM images of the products at different reaction time intervals were shown in Fig. 3, in which three obvious evolution stages could be identified. At first, solid ellipse particles of α-Fe_2O_3 were formed (Fig. 3a). When the reaction was conducted for 1 h, the solid nanoparticles became looser, and the dissolution occurred in the regions at the ends inside can be clearly seen (Fig. 3b). The dissolution primarily occurred at the ends inside, because the particles located in the ends inside have higher curvature and higher surface energy. As the reaction was prolonged to 2 h, the crystallites located in the surface of aggregates became larger, which may grow at the expanse of smaller crystallites inside through "solid-solution-solid" mass transportation, and the smaller crystallites would eventually dissolve into solution and regrow on the larger ones during Ostwald ripening process. Increasing reaction time to 4 h, the product was composed mainly of hollow spheres, with a continuously increasing cavity. Chen and co-workers have reported the existence of water can contribute to the dissolution–recrystallization process of α-Fe_2O_3.[33] In our system, the

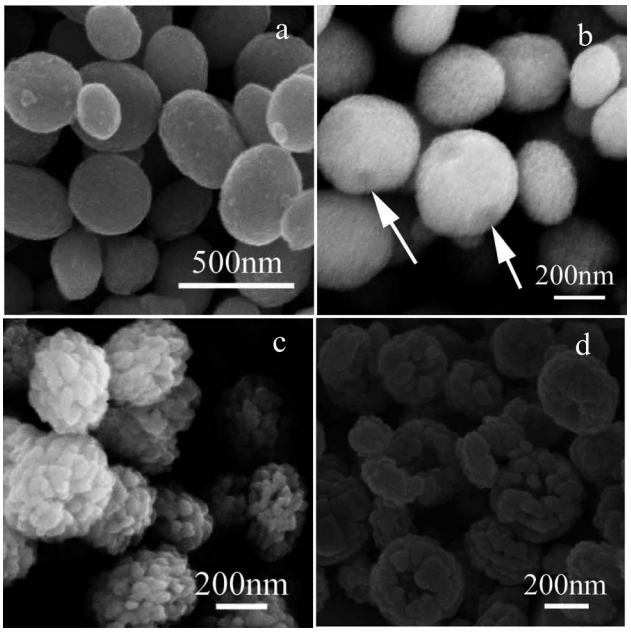

Fig. 3 SEM images of the products prepared with different reaction time. (a) 30 min; (b) 1 h; (c) 2 h and (d) 4 h.

dehydration of *n*-octanol will be occurred at the reaction temperature, which has been confirmed by our previous experiment by means of GC-MS.[35] The generated water molecules can be conducive to the dissolution–recrystallization process, and eventually leading to the synthesis of α-Fe_2O_3 hollow nanospheres.

Our experiment indicated that the amount of NaAc has an important role on the controlled synthesis of α-Fe_2O_3 nanostructures. With the amount of NaAc increasing the shell thickness of hollow spheres decreases, till the nanoflowers formed instead (shown in Fig. 2). With increasing the amount of NaAc, the pH and ionic strength of the solution increases, the mobility of the reactive ions and the formation of crystal nuclei decreases, which may eventually influence the morphology of the product. In fact, the inorganic species can be used as capping agents or structure-directing agents as their relatively small sizes may have important influence on the nucleation and growth process of product.[36,37] Meanwhile, Ac^- can chelate with Fe^{3+}, which can change the dynamics of the nuclei and growth rate of crystals, resulting in the oriented assembly of the product.[38] Furthermore, as an inorganic chemical additive, NaAc may have the effect of accelerating the ripening process through an enhancement in crystallite dissolution or chelating process, and realized the controlled synthesis of α-Fe_2O_3 nanostructures ultimately.[39]

As we known, solvent is important for the structure of the product, so the effect of solvent ratio on the formation of hollow products was also investigated (Fig. S1†). When the reactants were dissolved in pure ethanol without *n*-octanol while other conditions fixed, solid sphere aggregates and a large number of small nanoparticles were obtained (Fig. S1a†). And when only *n*-octanol was added, we still could not obtain hollow spheres (Fig. S1b†). This may be related to the solubility of the reactant: ethanol can increase the solubility of precursor, and the dehydration of *n*-octanol can contribute to the dissolution–recrystallization process of α-Fe_2O_3. The product has optimal internal void space and narrow range of sizes when the volume of *n*-octanol and ethanol was 12 mL and 8 mL respectively. As temperature is another important factor for the morphology of product, we carried out a series of experiments under different reaction temperature. When the reaction temperature was below 190 °C with other conditions unchanged, only solid product could be obtained (Fig. S2†). Hollow spheres could be prepared under a higher temperature over 200 °C. The results indicate that reaction temperature is crucial for the formation of hollow structures. At a temperature below the boiling point of *n*-octanol (195 °C), the dehydration reaction can not occur, as a result, hollow structures can not be formed, which is consistent with the results that we have obtained.

As a result, both reaction temperature and the solvent ratio of *n*-octanol and ethanol play important roles in the synthesis of hollow spheres, the amount of NaAc added was crucial on the controlled synthesis of α-Fe_2O_3 hollow spheres with oriented attachment.

Fig. 4 presents the nitrogen adsorption–desorption isotherm and the corresponding pore size distribution curve of the hollow α-Fe_2O_3 spheres in a typical synthesis. The hysteresis

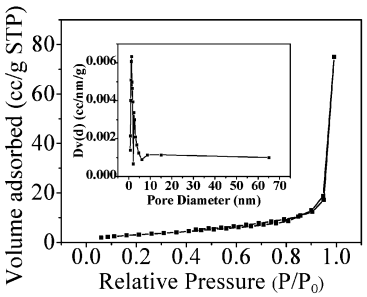

Fig. 4 Nitrogen adsorption–desorption isotherm and the corresponding pore size distribution curve for the hollow α-Fe_2O_3 spheres in a typical synthesis.

loop reveals the presence of mesopores with a relatively narrow pore size distribution in the synthesized hollow α-Fe_2O_3 spheres. The specific surface area of the hollow spheres calculated by the Brunauer–Emmett–Teller (BET) method is 12.2 $m^2 g^{-1}$, and the pore size distribution calculated from desorption branch by the Barrett–Joyner–Halenda (BJH) method is *ca.* 1.3 nm. Results indicated the formed hollow structure is affected by the amount of NaAc added, so nitrogen adsorption–desorption measurement was also carried out with adding different amount of NaAc. When 0.06, 0.12, 0.26 g of NaAc was added, the corresponding BET surface area was 6.7, 8.9, 10.1 $m^2 g^{-1}$, respectively (Fig. S3†), which is consistent with the TEM results that with the amount of NaAc increasing the formation of hollow wall decreases, till the hollow structures disappear.

The magnetic properties of synthesized α-Fe_2O_3 hollow spheres were investigated. As shown in Fig. 5a, the ZFC and FC curves are similar, and the samples we synthesized have a prominent Morin transition at 240 K (inset in Fig. 5a). As we known, bulk α-hematite has a Morin transition at 263 K,[32,40] our result is lower than the bulk α-Fe_2O_3 which may be caused by the dislocation-free structure and size effect in the sample.[26,41] Field-dependent magnetization measurements were carried out at 300 K in the applied magnetic field from −40 to 40 kOe. The magnetic hysteresis loop of α-Fe_2O_3 hollow spheres in Fig. 5b does not reach saturation up to the maximum applied magnetic field, and shows a ferromagnetic behavior with a high coercivity of 1785 Oe. Nanoparticles synthesized by various methods have different surface environment, microstructures *etc.*, which often

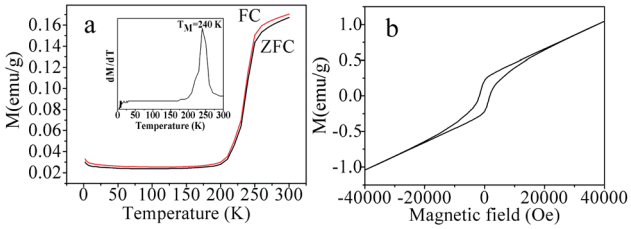

Fig. 5 Magnetic characterization of α-Fe_2O_3 hollow spheres in a typical synthesis. (a) Zero-field-cooling (ZFC) and field-cooling (FC) magnetization curves at the applied magnetic field of 1000 Oe. (b) Magnetic hysteresis loop at 300 K.

have a great influence on the magnetic properties of the nanoparticles. The relatively high coercivity may be caused by the shape anisotropy of the hollow nanospheres that do not fully close, similar to nanocup structures.[21,31]

The gas sensing properties of both as-prepared samples and commercial sample were investigated as shown in Fig. 6. It is well known that the response of a gas sensor is highly influenced by its operating temperature.[42] To determine the optimum operating temperature, the responses of the sensors (both the as-prepared samples S1–S4 and the commercial α-Fe_2O_3 powders S5) to 100 ppm ethanol were tested as a function of operating temperature. As shown in Fig. 6a, it can be clearly seen that the optimum operating temperature is nearly 290 °C for all samples.

To further examine the characteristics of the gas sensors, verify the superiority on the gas sensing properties of the as-prepared samples, we investigated the gas sensing property of commercial α-Fe_2O_3 powders in the same conditions. A bar graph of the responses of the five sensors toward eight types of gases was shown in Fig. 6b. All the gases were tested at an operating temperature of 290 °C with a concentration of 100 ppm. It is obvious that the sensors exhibited the highest response to acetone among the tested gases, and all the as-prepared samples S1–S4 showed higher sensitivity to each gas compared with the commercial sample S5. The dynamic response-recovery curves of the sensors to acetone vapor with increasing concentration were shown in Fig. 6d, which indicate the sensors have rapid response and good reversibility.[43] Gas responses of sensors upon exposures to different concentrations of acetone are displayed in Fig. 6c. There are significant differences among the sensors bases on the as-prepared samples and the commercial sample, which clearly show that the responses of the as-prepared samples are significantly superior to the commercial sample. For the samples S1–S5, the responses towards 1000 ppm of acetone gas reached 9.2, 11.9, 12.0, 10.1 and 3.6 respectively. As we known, the gas sensing properties of sensors are affected by many factors, such as size, morphology, surface area *etc.*[44] The higher responses of the as-prepared samples were mainly attributed to the higher special surface structure caused by their smaller particle size, which provided more active sites.[45] For the as-prepared samples S1–S4, the specific surface areas were 6.7, 8.9, 12.2, 10.1 $m^2\ g^{-1}$ respectively, which were mentioned above. The improvement of the sensing performance for samples S1 to S3 could be attributed to the increased surface area which caused by the different surface structures. For sample S4, the response was even lower than that of sample S2, which showed that surface area was not the only factor affecting the sensing performance. The different morphology of sample S4 (nanoflowers) compared to the samples S1–S3 (hollow spheres) also had an important influence on the gas sensing property.[46]

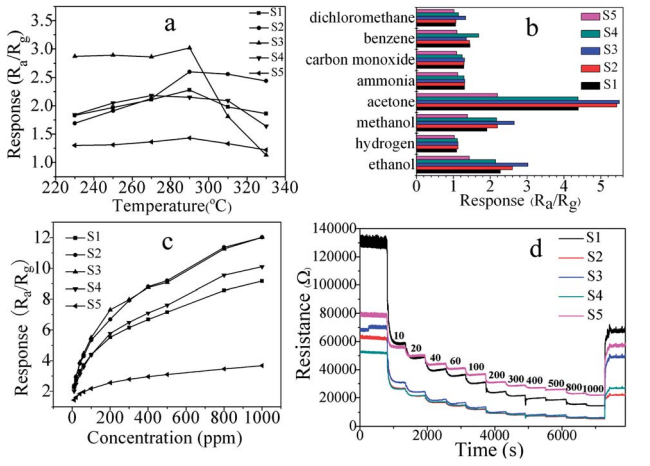

Fig. 6 (a) Responses of as-prepared samples S1–S4 with different amounts of NaAc: S1: 0.06 g, S2: 0.12 g, S3: 0.20 g, S4: 0.26 g and S5: commercial α-Fe_2O_3 powders at different operating temperatures, to 100 ppm ethanol vapor, respectively. (b) Responses of sensors to various gases (the concentration of all gases was 100 ppm). (c) Responses of the sensors to different concentrations of acetone vapor. (d) Time-dependent responses of the sensors to acetone vapor.

4. Conclusions

In summary, one-pot controlled synthesis of single-crystal α-Fe_2O_3 nanospheres was reported. The morphology was changed from hollow nanospheres to nanoflowers with increasing the amount of NaAc. In order to avoid the fast hydrolysis and polymerization problem of the iron ions, long-chain hydrophobic alcohols were used as solvents. Meanwhile, by making use of the slow dehydration of *n*-octanol, the dissolution–recrystallization of precursor would be facilitated and resulted in hollow nanostructures. This new strategy may gives us a new insight into the synthesis of other metal oxide nanostructures. Furthermore, the gas sensing property shows that as-prepared samples showed dramatically enhanced sensor sensitivity to acetone compared with the commercial sample, and the gas sensing behaviors were related with the morphologies and the BET surface area of the samples.

Acknowledgements

The work was supported by the National Natural Science Foundation of China (project no. 21201035, 21101028, 81371343), the Scientific and Technological Foundation of Fujian Province of China (project no. JK2013003), the Natural Science Foundation of Fujian Province (project no. 2012J05021, no. 2012J01204), and the Major Project of the State Ministry of Science and Technology of China (Project no. 2011ZX09101-001-04).

Notes and references

1 X. W. Lou, L. A. Archer and Z. C. Yang, *Adv. Mater.*, 2008, **20**, 3987.
2 K. An and T. Hyeon, *Nano Today*, 2009, **4**, 359.
3 M. M. Titirici, M. Antonietti and A. Thomas, *Chem. Mater.*, 2006, **18**, 3808.
4 Z. Zhong, Y. Yin, B. Gates and Y. Xia, *Adv. Mater.*, 2000, **12**, 206.

5 S. W. Kim, M. Kim, W. Y. Lee and T. Hyeon, *J. Am. Chem. Soc.*, 2002, **124**, 7642.
6 M. Yang, J. Ma, C. Zhang, Z. Yang and Y. Lu, *Angew. Chem., Int. Ed.*, 2005, **44**, 6727.
7 B. Wang, J. S. Chen, H. B. Wu, Z. Wang and X. W. Lou, *J. Am. Chem. Soc.*, 2011, **133**, 17146.
8 A. K. Ganguli, A. Ganguly and S. Vaidya, *Chem. Soc. Rev.*, 2010, **39**, 474.
9 M. J. Lawrence and G. D. Rees, *Adv. Drug Delivery Rev.*, 2012, **64**, 175.
10 X. L. Yu, C. B. Cao, H. S. Zhu, Q. S. Li, C. L. Liu and Q. H. Gong, *Adv. Funct. Mater.*, 2007, **17**, 1397.
11 H. Chen, J. He, C. Zhang and H. He, *J. Phys. Chem. C*, 2007, **111**, 18033.
12 Y. D. Yin, R. M. Rioux, C. K. Erdonmez, S. Hughes, A. G. Somorjai and A. P. Alivisatos, *Science*, 2004, **304**, 711.
13 Y. Xiong, B. Wiley, J. Chen, Z. Y. Li, Y. Yin and Y. Xia, *Angew. Chem., Int. Ed.*, 2005, **44**, 7913.
14 X. B. Cao, L. Gu, L. J. Zhuge, W. J. Gao, W. C. Wang and S. F. Wu, *Adv. Funct. Mater.*, 2006, **16**, 896.
15 X. W. Lou, Y. Wang, C. L. Yuan, J. Y. Lee and L. A. Archer, *Adv. Mater.*, 2006, **18**, 2325.
16 B. X. Li, G. X. Rong, Y. Xie, L. F. Huang and C. Q. Feng, *Inorg. Chem.*, 2006, **45**, 6404.
17 J. H. Yang, L. M. Qi, C. H. Lu, J. M. Ma and H. M. Cheng, *Angew. Chem., Int. Ed.*, 2005, **44**, 598.
18 S. W. Cao and Y. J. Zhu, *J. Phys. Chem. C*, 2008, **112**, 6253.
19 J. Chen, L. Xu, W. Li and X. Gou, *Adv. Mater.*, 2005, **17**, 582.
20 Y. Zheng, Y. Cheng, Y. Wang, F. Bao, L. Zhou, X. Wei, Y. Zhang and Q. Zheng, *J. Phys. Chem. B*, 2006, **110**, 3093.
21 X. L. Cheng, J. S. Jiang, M. Hu, G. Y. Mao, Z. W. Liu, Y. Zeng and Q. H. Zhang, *CrystEngComm*, 2012, **14**, 3056.
22 S. W. Cao and Y. J. Zhu, *Acta Mater.*, 2009, **57**, 2154.
23 P. Sun, Z. Zhu, P. Zhao, X. Liang, Y. Sun, F. Liu and G. Lu, *CrystEngComm*, 2012, **14**, 8335.
24 J. Zhu, Z. Yin, D. Yang, T. Sun, H. Yu, H. E. Hoster, H. H. Hng, H. Zhang and Q. Yan, *Energy Environ. Sci.*, 2013, **6**, 987.
25 S. Zeng, K. Tang, T. Li, Z. Liang, D. Wang, Y. Wang and W. Zhou, *J. Phys. Chem. C*, 2007, **111**, 10217.
26 S. Zeng, K. Tang, T. Li and Z. Liang, *J. Phys. Chem. C*, 2010, **114**, 274.
27 H. J. Song, X. H. Jia, H. Qi, X. F. Yang, H. Tang and C. Y. Min, *J. Mater. Chem.*, 2012, **22**, 3508.
28 Z. Wu, K. Yu, S. Zhang and Y. Xie, *J. Phys. Chem. C*, 2008, **112**, 11307.
29 Y. W. Jun, J. S. Choi and J. Cheon, *Angew. Chem., Int. Ed.*, 2006, **45**, 3414.
30 J. Zhong and C. Cao, *Sens. Actuators, B*, 2010, **145**, 651.
31 D. Jagadeesan, U. Mansoori, P. Mandal, A. Sundaresan and M. Eswaramoorthy, *Angew. Chem.*, 2008, **120**, 7799.
32 S. Zeng, K. Tang, T. Li, Z. Liang, D. Wang, Y. Wang, Y. Qi and W. Zhou, *J. Phys. Chem. C*, 2008, **112**, 4836.
33 J. Lu, D. Chen and X. Jiao, *J. Colloid Interface Sci.*, 2006, **303**, 437.
34 J. S. Chen, T. Zhu, X. H. Yang, H. G. Yang and X. W. Lou, *J. Am. Chem. Soc.*, 2010, **132**, 13162.
35 X. Jia, D. Chen, X. Jiao, T. He, H. Wang and W. Jiang, *J. Phys. Chem. C*, 2008, **112**, 911.
36 C. Wu, P. Yin, X. Zhu, C. OuYang and Y. Xie, *J. Phys. Chem. B*, 2006, **110**, 17806.
37 M. J. Siegfried and K. S. Choi, *J. Am. Chem. Soc.*, 2006, **128**, 10356.
38 X. L. Wu, Y. G. Guo, L. J. Wan and C. W. Hu, *J. Phys. Chem. C*, 2008, **112**, 16824.
39 H. C. Zeng, *J. Mater. Chem.*, 2006, **16**, 649–662.
40 J. H. Bang and K. S. Suslick, *J. Am. Chem. Soc.*, 2007, **129**, 2242.
41 D. Du and M. Cao, *J. Phys. Chem. C*, 2008, **112**, 10754.
42 P. Sun, X. He, W. Wang, J. Ma, Y. Sun and G. Lu, *CrystEngComm*, 2012, **14**, 2229.
43 X. Rao, X. Su, C. Yang, J. Wang, X. Zhen and D. Ling, *CrystEngComm*, 2013, **15**, 7250.
44 F. Li, J. Xu, X. Yu, L. Chen, J. Zhu, Z. Yang and X. Xin, *Sens. Actuators, B*, 2002, **81**, 165.
45 X. Li, W. Wei, S. Wang, L. Kuai and B. Geng, *Nanoscale*, 2011, **3**, 718.
46 H. J. Song, X. H. Jia and X. Q. Zhang, *J. Mater. Chem.*, 2012, **22**, 22699.

